

TANGO ARRAY

An Air Shower Experiment in Buenos Aires[†]

P. Bauleo, C. Bonifazi, A. Filevich¹ and A. Reguera²

*Departamento de Física, Comisión Nacional de Energía Atómica,
Avenida del Libertador 8250, (1429) Buenos Aires, Argentina*

Abstract

A new Air Shower Observatory has been constructed in Buenos Aires during 1999, and commissioned and set in operation in 2000. The observatory consists of an array of four water Čerenkov detectors, enclosing a geometrical area of $\sim 30.000\text{ m}^2$, and is optimized for the observation of cosmic rays in the “knee” energy region. The array detects ~ 250 to ~ 1500 showers/day, depending on the selected triggering condition. In this paper, the design and construction of the array, and the automatic system for data adquisition, daily calibration, and monitoring, are described. Also, the Monte Carlo simulations performed to develop a shower database, as well as the studies performed using the database to estimate the response and the angular and energy resolutions of the array, are presented in detail.

[†] Further information available in <http://www.tango-array.org>

¹ Fellow of the CONICET, Argentina.

² Now at Telesoft S.p.A., Buenos Aires.

1 Introduction

The Earth's atmosphere is being bombarded continuously by a flux of particles (cosmic rays), coming from all directions. Their energies range from a few MeV to more than 10^{20} eV. Their spectrum follows a power law with a negative exponent which is almost constant over thirteen orders of magnitude in energy. The origin of the cosmic rays is still an open question. Those rays with energy below ~ 1 GeV are likely to have a solar origin, but for higher energies their acceleration mechanism remains in mystery. It is believed that up to $\sim 4 \cdot 10^{15}$ eV they can be accelerated by diffuse shock processes produced in supernova explosions. In this energy region, (usually called "the knee"), the exponent of the power law describing the cosmic ray flux per units of area, time, solid angle, and energy, suddenly steepens from ~ -2.7 to ~ -3.2 , and this change is believed to be related with the maximum energy that can be transferred by a supernova shock to a single particle. If the kinetic energy of the cosmic ray is high enough, then secondary particles are produced as a consequence of hadronic or electromagnetic interactions with the upper atmosphere atomic nuclei. Those secondary particles will, in turn, produce more particles, yielding a cascade which is known as an Extensive Air Shower (EAS). Depending on the primary energy and zenithal angle, this cascade can be stopped in the atmosphere, or even reach the ground level.

A method which has been used for the observation of EAS is the detection of the light emitted by the Čerenkov effect in air, while fast charged particles, (mainly electrons), are crossing the atmosphere (WHIPPLE, CANGAROO). Alternatively, it is possible to observe the UV light emitted by decay processes occurring in the atmospheric molecules after excitation by the EAS's secondary particles (Fly's Eye, HiRes, Pierre Auger Project, Telescope Array, OWL Project). The amount of UV and Čerenkov light emitted by an EAS is extremely faint, and because of this it is possible to observe these processes only during moonless dark nights, and by using relatively large telescope mirrors as light concentrators and sensitive photomultiplier tubes.

Another (and perhaps more common) approach (Haverah Park, AGASA, Volcano Ranch, SUGAR) is the direct detection of the shower secondary particles reaching the ground level. The size of the footprint at ground level is several thousand square meters for showers produced by primary cosmic rays of energies near the "knee" or higher. Because of this these experiments are designed so as to observe only samples of the particle showers using an array of ground-based detector stations, where gas-filled chambers, plastic scintillators or Čerenkov-effect detectors are typical components.

The detector stations of these ground arrays are usually capable to measure particle densities. In the case of the array described in the present work, where water Čerenkov detectors (WCD) are used, this measurement is performed through a sample of the amount of light emitted when the shower particles traverse through the water radiator. Also, the precise relative times of the signals produced by each station are recorded, together with the Čerenkov light intensity information. By using the relative hitting times at each station and the known geometry of the array it is possible to determine the direction of arrival of the primary cosmic ray, assuming that the general development of the shower follows a rather flat front profile. Rigorously the shower front is a curved surface whose radius of curvature

could in principle be determined if the number (and quality) of the sampling detectors is high enough.

The determination of the primary energy from EAS measurements using ground-based detectors is closely tied to shower reconstructions, based on Monte Carlo simulations. These simulations correlate the primary energy to the particle densities at a fixed distance from the shower “core” position, that is, the center of gravity of the air shower at ground. In a simplified model, the primary energy is simply estimated as a magnitude proportional to the total number of particles in a shower. Hence, the particle density measurements performed by each station is used to estimate the total number of particles of the shower.

In the following sections the design and construction of this new air shower experiment, which has been optimized for the “knee” region of the energy spectrum, are described. The necessary simulations, which were required to set the numerous design parameters of the array, are presented in detail.

2 The array

The TANGO (**T**ANdar **G**round **O**bservatory) Array has been constructed in Buenos Aires, Argentina, at (~ 15 m a.s.l), $35^\circ 34' 21''$ S and $58^\circ 30' 50''$ W, in the Campus of the Constituyentes Atomic Center, belonging to the Argentinean Atomic Energy Commission (CNEA). The data acquisition (DAQ) room was set inside the TANDAR Accelerator Building. Three detectors are placed on the vertices of an almost isosceles triangle, and a fourth detector was installed on top of the building, in a convenient position close to the center of the triangle, as shown in Figure 1. The final positions of the detector stations were conditioned by the free space available between the existing buildings, and an effort was made to come up to an overall shape as close as possible to an equilateral triangle, which maximizes the effective collection area. The distances between surface stations were measured using a GPS and their error has been estimated in ± 1 m (the measurement was performed after release of the high precision GPS service). The final configuration encloses a geometrical area of 31286 m^2 . The array has a yearly average overburden of $\sim 1000\text{ gr/cm}^2$.

During an EAS event the DAQ system measures both, the intensities of the Čerenkov photons emitted by the water when crossed by the secondary particles of a high energy cosmic ray’s EAS, and also, the arrival time of the these particles to each station. The threshold energy of the array, resulting from the geometry and from the particular detector conditions, (present noise, trigger levels, etc) is close to 10^{14} eV for vertical showers. The detector stations are connected by low attenuation (RG-213) coaxial cables to the DAQ room, where the signals are recorded using a 4-channel digital oscilloscope connected to a computer. Depending on the selected trigger conditions, which are generated by standard NIM electronic modules, the number of accepted events ranges from ~ 250 to ~ 1500 per day.

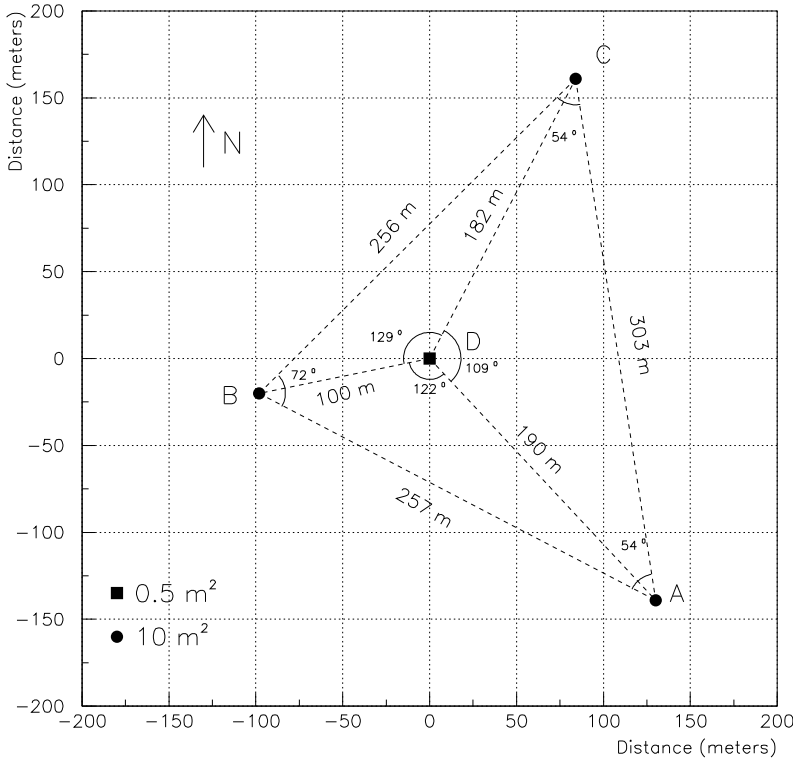


Figure 1: TANGO Array Layout. Circles indicate the positions of the three 10 m^2 stations, whereas the square shows the position of the central, 0.5 m^2 detector. The distances shown in the figure have been measured using a GPS.

2.1 The detector stations

This array is a project which grew up from the first 1:1 scale prototype of a WCD [1](See Figure 2) built in 1995 by members of the local Pierre Auger Project Collaboration [2]. This first detector (labelled A in Figure 1) was constructed in a tank, cylindrical in shape, made of 0.68 mm stainless steel plate, with a footprint area of 10 m^2 . The effective water depth is 120 cm. Three, 8-inch photomultipliers (Hamamatsu R1408), symmetrically placed at 120 cm from the tank axis were installed looking down on the top of the detector, having only the photocathodes immersed in the water working as Čerenkov radiator. Thus, a sample of the Čerenkov photons emitted when a charged particle crosses the tank are collected by the three PMTs. This detector, being a prototype, was designed as a flexible system, allowing the introduction of modifications in the photomultiplier positions, the effective water height, or the inner lining material. During the measurements as a component of the TANGO array the configuration of this detector was that of the Pierre Auger Project baseline design[2], with the dimensions mentioned above. In order to improve the optical properties of the inner surfaces all detectors were fully lined with Tyvek which is a highly UV-diffusive and reflective material[4].

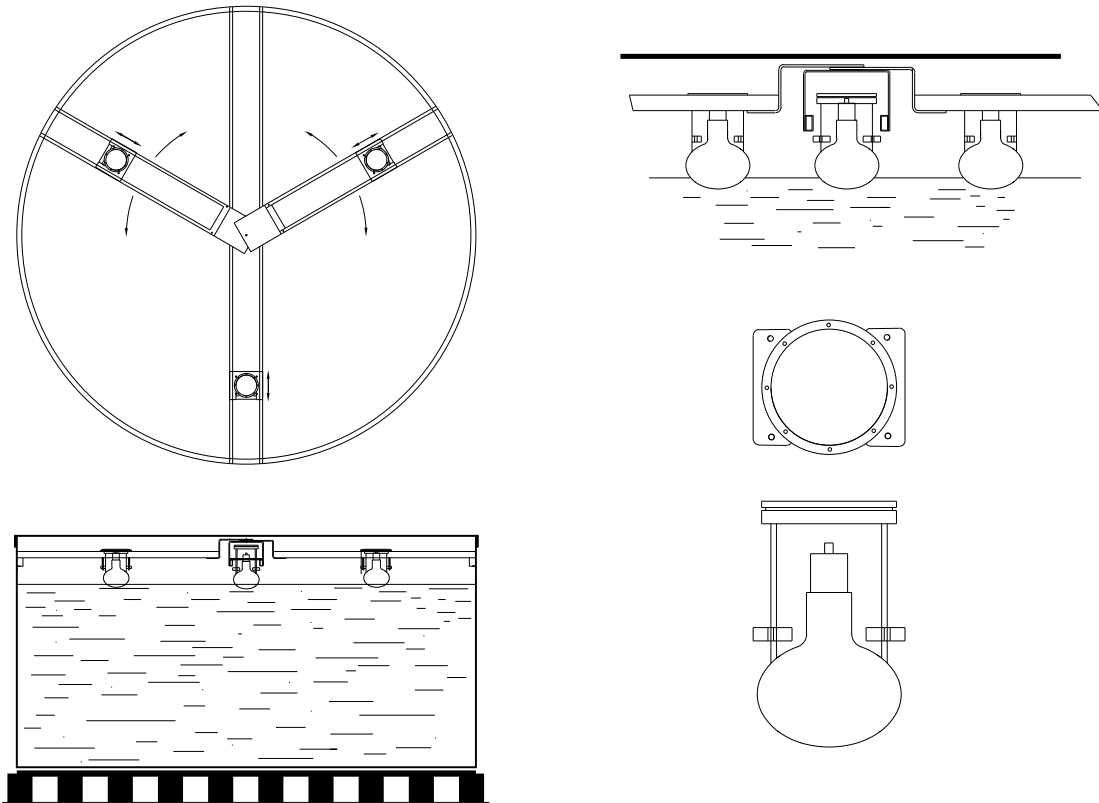


Figure 2: Top and side view of the first 10 m^2 detector used in the experiment. In the right is shown a detail of the PMT's enclosure.

The two other detectors sitting in the vertices of the triangle (B and C in Figure 1) have the same general dimensions quoted previously. They are made of 1 mm thick stainless steel, and the external walls are shaped as a dodecagon (see Figure 3). In these detectors we used Hamamatsu R5912, 8-inch diameter PMTs, arranged with the same geometry used in the first detector tank. The fourth detector (D) is smaller, it was made using a fiberglass-reinforced polystyrene tank, with a footprint of 0.5 m^2 and an effective water depth of 80 cm. The tank was also internally lined with Tyvek and only one, 3-inch PMT, was installed centered on the top of the tank.

The larger outer detectors are more adequate to measure lower particle densities generated by showers falling relatively far away from them, either close to the center of the array or very away the whole array. The relatively large ratio between the volume of the external detectors to that of the smaller central detector helps to improve the accuracy in the determination of the particle densities in those cases where the shower core falls close to the center of the array. This is so because of the larger dynamic range of the central detector, which admits higher particle densities without going into saturation (See Section 2.3, and the higher sensitivity of the larger detectors placed on the vertices of the triangle.

All PMTs used in the WCDs were mounted in water-tight enclosures that protect from moisture their voltage dividers and only the photocathode areas of the glass bulbs are immersed in the water radiator (See Figure 2. The glass bulbs of the PMTs were glued to the



Figure 3: Detector B. The cabinet installed on the wall at the right side contains the local electronics and the high voltage power supply.

PVC housings using an elastic silicone compound to reduce mechanical stresses that could break the glass, as happened in the Milagrito experiment[3]. Local high voltage power supplies, fed from the AC mains, were installed near each station. The bias configuration of all PMTs was adopted as grounded cathode, to prevent eventual noise produced by electrical leaks or discharges through the glass.

The water used to fill the tanks was treated in a reverse-osmosis plant, producing an average final water resistivity of about $1 \text{ M}\Omega\text{-cm}$. Before filling the tanks they were carefully degreased, brushed with water and mild detergent and rinsed abundantly with the same water used as the detector material. These precautions, together with the darkness and the fact that the water used as detector material has a very low level of bacteria nutrients, virtually blocked any extensive biological activity [5]. After more than 1 year since the filling of the detectors, no significative decrease in the signal strength has been observed.

2.2 Characterization of the photomultiplier tubes

The gains of the three (R1408) PMTs used in the first prototype were measured previously[6], and we have built a dark box, adequate for measuring the gain and dark current of the new Hamamatsu R5912 tubes, purchased for the new detector stations. We also used this darkbox to characterize the photocathode sensitivity profiles and the influence of the Earth magnetic field direction of the PMTs. The dimensions of the box are $50 \times 50 \times 100 \text{ cm}$ and accepts one PMT, which is mounted in an axially rotatable holder.

Using electrons thermally emitted from the photocathodes at room temperature, we measured the gains of the PMTs by means of the single electron technique. In these measurements we tested different voltage divider configurations in a range of high voltage from 1100

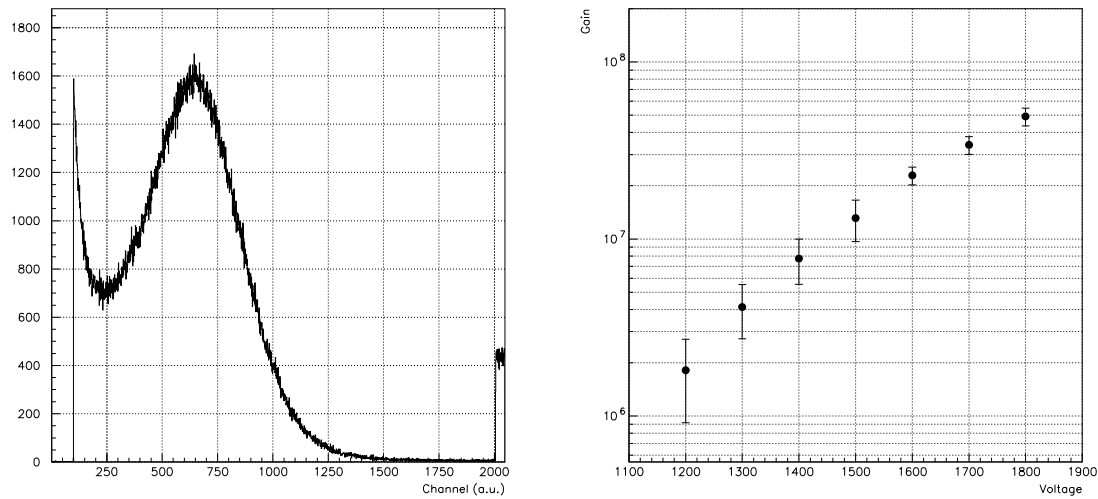


Figure 4: Typical single electron spectrum measured at 1500 Volts (left) and gain (right) for a Hamamatsu R5912 tube measured using the dark box.

to 1800 V. In all cases the tubes were kept in total darkness for at least 2 hours before collecting the single electron spectra, to reduce the rate of multi-electron emissions due to fast decaying fluorescence in the photocatodes. The dark current pulse rate (threshold = 1/3 p.e.) after one hour of storage in total darkness was about 900 Hz at 1500 Volts. A typical spectrum and a plot of the gain values are shown in Figure 4.

A study of the influence on the PMT gain of the Earth magnetic field direction relative to the dynode geometry, was also performed. The gains were carefully measured at a fixed HV setting (1.5 kV) for 8 different azimuthal orientations of the PMTs, covering 360° . The tubes were measured keeping always their axis in vertical position. No significative shifts (less than $\pm 1\%$) were observed in the peak positions of the single electron spectra obtained in this way. From these results we concluded that the local influence of the Earth magnetic field direction on the gain can be neglected, and thus no special care was taken to install the tubes in the detector stations at any special dynode orientation.

2.3 Gain settings and calibration of the detector electronics

After testing several possible configurations we adopted a passive, grounded cathode design for the voltage dividers, as simple and reliable as possible, assuring both wide dynamic range, and linearity. The final configuration chosen is similar to that recommended by Hamamatsu for the R5912 tubes. Metal film resistors were used, and decoupling capacitors stabilize the 3 last dynodes. The finished printed cards were protected with water resistant varnish and installed with bags of dessicant material in the water-tight enclosures mentioned above.

It is important that the gains of the 3 PMTs installed in each detector station are matched to each other to avoid unbalances in charge collection. Unmatching could impair the ho-

mogeneity in the response of the detector, and even reduce the dynamic range. Because of availability of equipment and space, we used a common high voltage supply in each detector station. Because of this, and provided that the observed differences in gains were small (less than 15 %), we compensated the differences in gain by using passive, constant-impedance variable attenuators to reduce as necessary the output pulse amplitude of the two tubes having larger gains in each station.

In order to determine the relative gains we adopted a routine procedure based on the measurement of the signal from each PMT produced by background muons. The trigger for this measurement is taken from the signals from other PMT belonging to the same station, as described in[7]. Once the average relative gains are obtained for the three tubes, the attenuators are set in the two PMTs with higher gains, matching the peak position produced by the PMT with lowest gain. This procedure for gain matching and calibration has been performed on a monthly basis during the complete period of measurements. The system proved to be very stable and very few adjustments were required along this time.

In addition to this periodic gain matching monitoring procedure, a daily routine for monitoring the overall gain of the 4 detector stations has been performed. It also uses the natural background muons falling in the detectors as the source of signals for calibration. It has been found that the spectra of the summed signals of the three PMTs within each peripheral detector station, and also the response of the 3" PMT installed in the small central detector show clearly a peak when they are triggered by themselves. Although it is somewhat broad, the position of this "background" muon peak is very closely the same as the position of the similar peak obtained when a pair of external plastic scintillators are used to select vertical and central muons for triggering. This is valid for both, voltage and charge spectra. This experimental result, which might be due to the remarkable uniformity in the light distribution produced by the Tyvek liners, provides a simple and reliable procedure for remote monitoring and calibration of the station gain [8]. This peak value has been called VEM (**Vertical Equivalent Muon**), and is defined as the charge (or voltage) peak produced by singly charged, energetic particles, crossing vertically the detector along its axis. This VEM-value is a characteristic parameter of each detector, and depends on its components, geometry, construction, and also on its operation conditions (transparency of the water radiator, bias voltage, etc). The VEM-value provides a practical way to normalize the signals from different detectors and moreover, to express the total signal produced in each station by an EAS (*i.e.* muons, electrons, gamma rays, etc., hitting the station) in terms of an "equivalent reference particle". Muons have been selected in this case as they are present everywhere and proved to be very convenient for calibration.

In previous studies[9] performed with the prototype detector, very good homogeneity in charge collection was obtained by using the sum of the signals of the three PMTS. This behavior, which might be again attributed to the excellent light spread produced by the Tyvek liners, is kept almost independently of the entrance points and directions of the muons.

According to these results, our design included fast active adder circuits installed in the peripheral detectors. The operational amplifier employed (CLC 452) works also as the driver for the relatively long RG-213 cable, carrying the signals from each detector to the DAQ

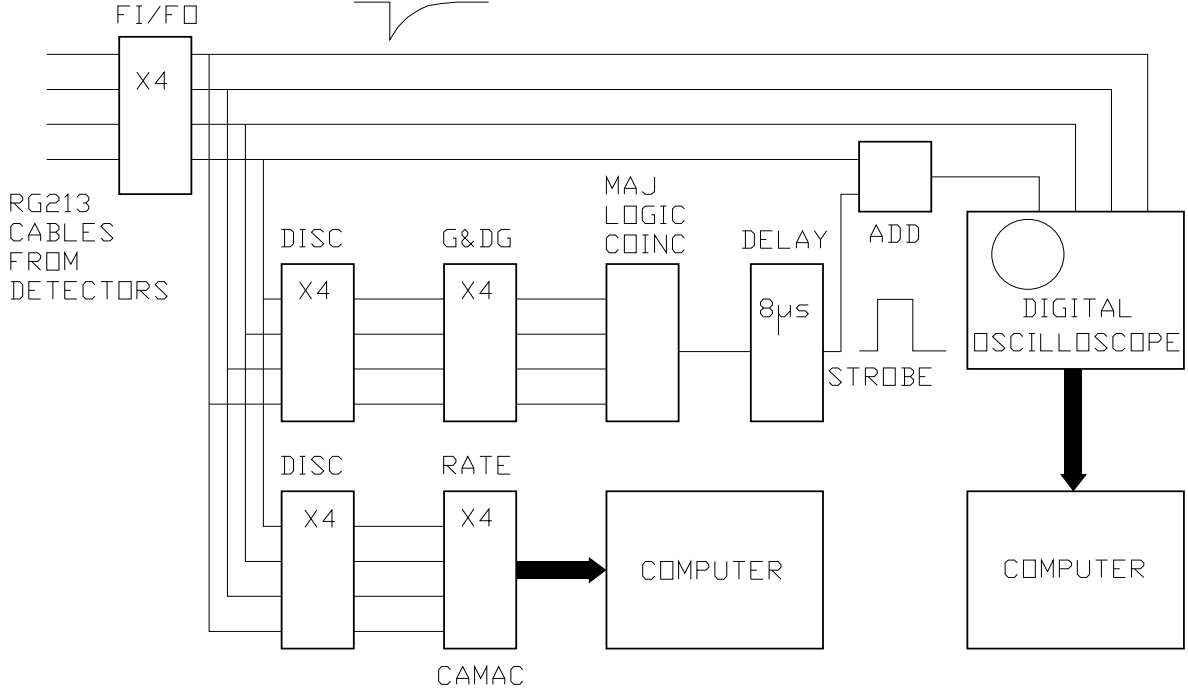


Figure 5: Simplified block scheme of the Trigger and DAQ system.

room. Although their response in speed is excellent (we require a 130 MHz bandwidth), these circuits introduce a limitation in the dynamic range as the maximum span voltage is less than 2 V. In order to reduce the reflection of the pick up noise signal the impedance of the cable was matched at the sending end, but this reduces further the available amplitude to only 1.4 V. On the other hand, an acceptable signal to noise ratio in the DAQ room asks for minimum signal amplitudes for single muons of ~ 100 mV. These figures, together with the measured RF pick up and the signal attenuation produced along the cables, limit the final available dynamic range from 1 to 15 muons. Even when this dynamic range is limited, it has been found to be acceptable because only $\sim 30\%$ of the events had to be rejected in the off-line data analysis due to electronic saturation in any station.

Because there is only one PMT in the central detector, and the cable length to the DAQ room is relatively short (~ 45 m), its anode signal was directly sent without summing circuit nor attenuator, and hence without the limitation in the dynamic range present in the outer detectors.

2.4 Trigger System and Data Acquisition

The signals from the four stations arriving to the electronics front panel are split using linear fan-in/fan-out (FIFO) modules (see Figure 5). Then, they are fed directly to the input connectors of a four-channel digital oscilloscope (Tektronix TDS 3034 set at 500 Ms/s). The oscilloscope is the core of our DAQ system and works as the digitizing stage for detector signals under control of a STROBE pulse. The detector signals are at this point unsyn-



Figure 6: Data Acquisition Room. The core of the DAQ system is the digital oscilloscope. On the right can be seen the cables connecting the DAQ room with the detectors.

chronized after travelling different lengths of cables (206, 196, 310 and 44 m, for detectors A,B,C,D, respectively). Thus, in order to generate valid trigger conditions, it is essential to compensate these different transit times. With this purpose, we use the second signals from the FIFOs to generate logical pulses in analog discriminators (discrimination level ~ 1 VEM), then these pulses are delayed accurately to compensate for these differences in time and then they are fed to a majority logic coincidence unit to select the desired trigger condition. The time window in this module is set to $1.1 \mu\text{s}$, covering safely the maximum time used by the EAS front to go across the array, even for the case of almost horizontal directions.

The digital oscilloscope available does not feature external trigger. For this reason one of the analog channels had to be used for triggering purposes, in addition to its signal digitizing function. With this purpose the STROBE signal generated by the coincidence unit, indicating the production of an event of interest (in practice 3 or 4-fold coincidences) is delayed about $8 \mu\text{s}$ after arrival of the last detector signal and then summed to one of the detector channels (channel 4 in Figure 5 and 7). Because of the relatively low singles counting rates and with the introduced delay of $8 \mu\text{s}$ no overlaps are produced in practice. Provided that the STROBE pulse is summed with opposite polarity respect to the detector signals the Advanced Trigger feature of the oscilloscope could be safely used for triggering.

When the STROBE pulse is detected by the oscilloscope, the SAVE procedure is initiated, *i.e.*, the traces stored in the four channel memories corresponding to the last 16384 ns, are frozen and transferred to the PC disk. This time slice allows us to obtain a good measurement of both, the desired detector signals and the unavoidable radio noise pick-up in the long cables carrying the signals.

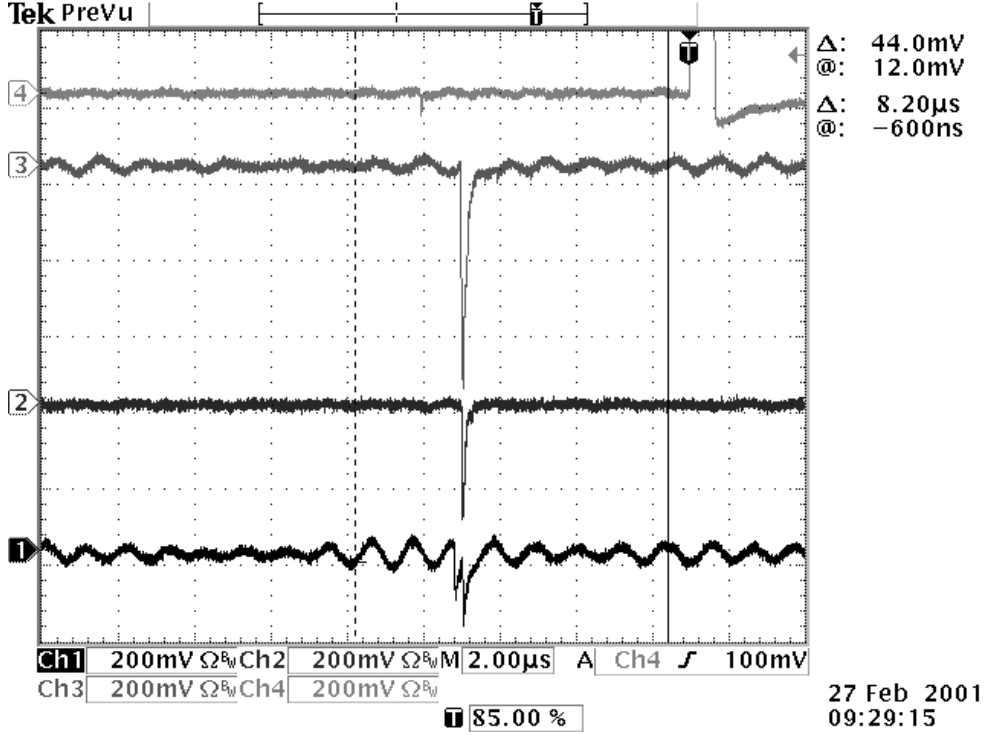


Figure 7: Oscilloscope screen during the capture of a real shower. In channel 4 the STROBE signal is summed (with positive polarity) to the signal from detector D and indicated with the symbol “T” (trigger). In the time region between cursors (8 to 16 μ s) the signals from a typical shower can be observed. The individual traces has been vertically shifted for clarity.

The system dead time (digitalization, data transfer and PC storage) is 22 seconds for event. This relatively long dead time is primarily produced by the transfers, through the RS-232 serial port working, at 19200 bps. This dead time is considered acceptable in comparison with the average time between events, which is of the order of 6 minutes.

The first time region of 8192 ns (up to the first cursor in Figure 7) is used to compute the bias level at the time of presentation of the detector signals. The typical pick up noise appears as a dominant oscillation with a period of the order of 1 μ s, corresponding mainly to the AM broadcasting stations. The following 8192 ns region, between the cursors, is the time region where the detector signals are stored. The last region which contains the STROBE signal is not saved to disk. The internal 150 MHz bandwidth low-pass filter built in the oscilloscope is active in order to reduce the amplitude of higher frequency signals. A fast Fourier analysis of the detector signals indicated that their main harmonic components extend up to ~ 100 MHz, thus little distortion in the detector signals is introduced by the filter.

A special program was written to drive the data acquisition system in a completely automatic way. Normal collection of shower events is performed when the program runs in “Survey Mode”. The detection of a STROBE pulse causes that the oscilloscope traces recorded in the 4 channels are saved to disk, together with information on the year, day, and local civil time, which allows to reconstruct the equatorial or galactic coordinates of the shower arrival direction.

In addition, every day the program switches at a predetermined time to the “Calibration Mode”. In this mode, the collection of data from each detector station is self-triggered, in order to record background events to calibrate the stations, *i.e.* to determine the daily VEM value for each station. The four detectors are measured sequentially in this mode, under program control. The data are stored to disk and analyzed off-line. Roughly, one hour and a half is required to acquire 3000 background events (found to be adequate to obtain the VEM values with an error of $\sim 5\%$) for each station and to save the calibration data from the four detectors. The starting time for the calibration procedure, and the total amount of background events for each detector, are set in an ASCII file. Once the calibration is completed, the program automatically switches to the “Survey mode” described above. This mode of operation is kept until the “Calibration Mode” is called up again, at the programmed time next day.

The singles counting rates of the four detector stations are permanently recorded using a CAMAC scaler with a refreshing time of 1 s, and are also saved to disk. This information is valuable for monitoring the status of each station. It helped discarding particular data when the operating condition of a particular station became unstable due, for instance, to a high level of pick up noise, or gave an alert signal for the need of maintenance of a station, in occasional cases of light leaks. The recording of the counting rates is also program-controlled and does not require operator action to run, once it is launched.

3 Simulated performance of the array

In order to characterize the behavior of the array, detailed simulations were performed to estimate its efficiency for shower detection and its angular and energy resolutions. A special routine, simulating the detector response to the different shower particles, has also been written to provide an input for the reconstruction routines.

3.1 Shower database

The AIRES program [10] using the SYBILL hadronic package was used in the first step of the simulation pipeline: the construction of an adequate shower database containing detailed information about the secondary particles at ground produced by primary cosmic rays of the energies of interest.

The shower simulation starts with the injection of a primary particle in the high atmosphere (~ 100 km above sea level) and tracks down the different generations of secondary particles in the subsequent cascade. The technique known as *thinning*[10] was used to reduce the CPU time and the disk storage requirement. This procedure consists in tracking explicitly all particles above certain energy threshold (or *thinning* energy), and those particles having an energy level below the threshold are computed using statistical weight. In our simulations we set a relative thinning energy level of 5.10^{-5} with respect to the primary particle energy.

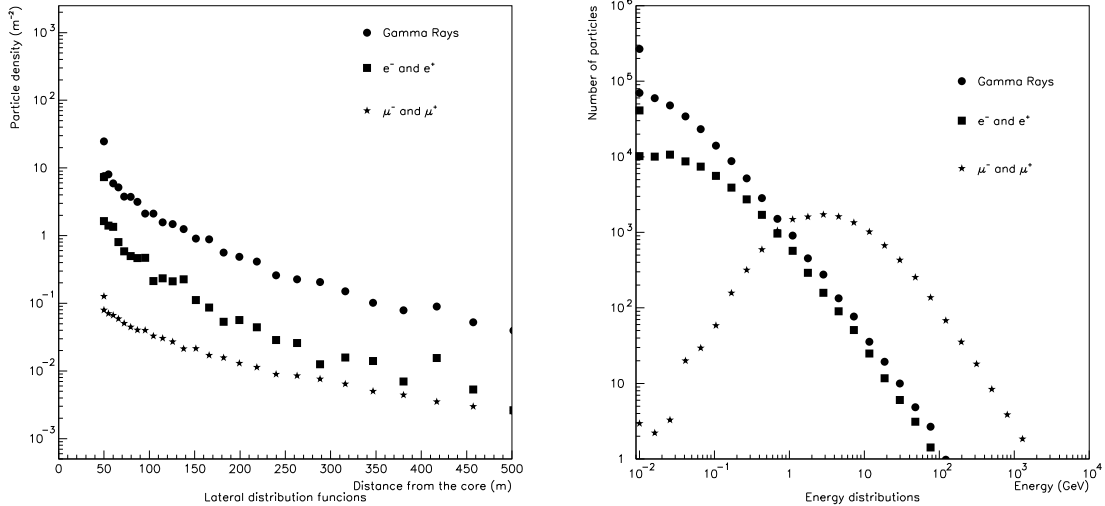


Figure 8: Lateral distribution function and energy distribution for different particle species in the cascade. These distributions corresponds to a proton primary of 2.10^{15} eV and a zenithal angle of 30° . These curves are typical AIRES results.

To construct the shower database, twenty primary energies ranging from 10^{14} eV to 10^{18} eV were selected, and two nuclear species (protons and iron nuclei) were considered as primary particles. They were injected at zenithal angles from 0° to 60° , in 15° steps. To reduce the artificial fluctuations due in part to the thinning method [11], and also to obtain representative values of the relevant parameters, batches of 100 showers were simulated under the same initial conditions (as described above), and their average and RMS values were used. All these simulations were performed considering a ground level of 15 m.a.s.l.

The AIRES program produces a set of tables written in ASCII code, in which the information referent to the secondary particles reaching ground level (after deconvolution of the thinning algorithm) can be expressed simply as particle densities as a function of the core distance. This function is called *lateral distribution function* (LDF). In addition, for those particles “reaching” the ground level, these tables provide the landing time as function of the shower core distance and also their energy distribution. These tables include the mean, RMS and extreme values for each computed variable bin.

Figure 8 shows a typical example of AIRES results for the LDF and for the energy distributions produced by a proton primary of 2.10^{15} eV impinging at a zenithal angle of 30° .

Thus, by running protons and iron nuclei as primary particles, the AIRES database contains an amount of 20000 simulated showers covering the energy and zenithal range of interest for the TANGO Array. The shower database tables contains only particle densities, energies and arrival times (with respect to the core position particles arrival times) for muons, electrons, and gamma-rays.

3.2 Array simulation procedure

In order to predict the response of the array, the information on showers contained in the AIRES database tables was used to simulate events, *i.e.* the effect of individual showers falling relatively close to the array.

A simulated shower is a set of information describing in detail the calculated number and properties of secondary particles reaching the ground level. A simulated event is the set of information about the calculated effect of the shower on the array, taking into account the simulation of the detector, DAQ hardware, electronics, etc. With this purpose the showers are read from the AIRES database tables, establishing the number, energy and type of particles hitting each detector station, and their relative arrival time. The result of an event is a set of electronic signals from the detectors which are stored in computer memory. The simulation of each particular event allows to determine if it triggers or not the DAQ system. A total number of 360000 “events”, including all primary species and energies have been simulated from the information contained in the AIRES tables and they constitute the *simulated events database*. The procedure to simulate one event is described as follows:

- For each primary energy, 9000 shower core positions were selected landing at random in a area larger than the geometrical area of the array. In this way we can estimate the effect of showers falling outside the boundaries and obtain an estimation of their triggering efficiency. The size of this landing area was scaled logarithmically with the primary energy with the purpose to take into account the increase of the shower size at ground with energy.
- For each core landing position the zenithal and azimuthal angles of the event were chosen as follows: the azimuthal angle was uniformly distributed, and the zenithal angle distribution can be described by a $\cos^3(\theta)$ function, with a cut-off at 45° . This cut-off was selected accordingly with the atmospheric depth at Buenos Aires, where most EASs arrive within a cone of $\sim 40^\circ$. The exponent of the distribution was chosen so as to produce a distribution flatter than the flattest one reported up to date [3]. This was done with the purpose of including in the database a number statistically significant of simulated events at higher zenithal angles.
- Once the event core position and the angles were established for each particular event, the distances from each detector station to the core were calculated. Then, from the AIRES tables the apropiate mean values and dispersions were extracted and interpolated to reproduce the simulated event.
- To include the shower-to-shower fluctuations, uniform random number generators were profiled (using the accept-reject technique) [12] to reproduce the mean value and dispersion of the AIRES particle density tables contained in the database, according to the particular secondary particle considered. With the AIRES tables interpolated to the particular conditions of each simulated event, and the modified random number generators, the densities (particles/m²) of muons (both charges), electrons (both charges) and gamma-rays hitting each detector neighbourhood, were obtained. Finally, these

density values were scaled according to the geometrical area of each detector to obtain the number of particles falling over each detector in each shower.

- The energy and arrival time of every individual particle hitting each detector station were obtained using the same procedure (the accept-reject technique). This was made taking by into account the particle species and its distance to the core.
- Once the number of particles, energies and arrival times of all particle species falling on each station for the event, were obtained, the detector signal was obtained as is described in detail in 3.2.1.
- The next step in this calculation was the simulation of the response of the data acquisition electronics by performing a check to determine whether each particular simulated shower produces or not a valid trigger. With this purpose, the simulated traces for each detector station were scanned, searching for the threshold crossing times in each channel (there could exist multiple crossings in a single event). Then, these threshold crossing times, determined in each channel, were compared to those corresponding to the other channels to establish the presence of temporal coincidences between the traces (an EAS). If multiple crossing times were present in one or more channels, each one of them was searched for time coincidence with the other channels. The threshold levels in all channels were set as equivalent to the signal amplitudes produced by 1 VEM from each particular detector, and the time window for the coincidences was set to $1.1\mu\text{s}$, in correspondence to the real situation during measurements. If a coincidence condition was found, then the event was classified accordingly to the number of stations involved in the coincidence.
- Finally, the behavior of the A/D converter stage was also simulated, featuring a FADC working at 500 Ms/s (like that used in the data acquisition system). An appropriate noise generator has been included. From noise spectrum measurements we concluded that the local AM radio stations are the main noise sources, contributing with ~ 15 to 30 mV to the signal (the typical signal amplitude corresponding to one single particle is ~ 100 mV). The noise spectrum can be described as a continuous distribution with superposed, strongly varying peaks corresponding to the well-known local AM broadcasting frequencies, ranging from ~ 550 to ~ 1650 kHz. The FM band is also seen in the noise spectrum. However, its amplitude is much lower and can be safely ignored. On this basis, in order to obtain a realistic simulation, we added to the simulated signals a noise spectrum which follows the description given above.

All computer programs required for the simulation pipeline (except AIRES) were especially developed in the present work.

3.2.1 Detector simulation

A simple and very fast simulation program was written to emulate the detector response. In this program, instead of simulating in detail the production and transmission of the Čerenkov photons emitted during the passage of charged particles through the water, we

used the detailed knowledge of the detector behavior achieved during the previous years of operation of the first prototype. On this basis, the detector response was reproduced accordingly to a large set of measured parameters. In the following, prior to describing the detector simulation program, we present a summary of the experimental data, obtained previously.

In previous experiments [1, 13] the response of the WCD to vertical and tilted muons has been observed in detail. In these experiments, the entrance and exit points of the muons on the detector surface have been carefully selected to cover as much as possible all possible situations. A total of 38 different particle track lengths have been measured, corresponding to 162 different situations derived from the symmetry properties of the detector configuration. A particle track is considered to be “fully contained” when the entrance point of the muon is anywhere on the lid and the exit point is in the bottom, or when the entrance and exit points are near diametrically placed on the lateral cylindrical wall of the detector. Either an entrance or exit point on the side wall, and the other in the bottom or in the lid, are considered to produce a “clipping corner” track. As a result of these measurements (which are summarized in the Figure 9) we have found that the sum of the charges collected in the three PMTs of our WCD is, very approximately, directly proportional to the track length of the particle in the water radiator, and this is valid regardless of the entrance point position or the zenithal angle of the track.

For all measured tracks the digitized pulse shapes were recorded. The rise and fall times remain almost constant for the whole range of track lengths, which might be understood from the fact that these parameters are primarily determined by the highly diffusive properties of the Tyvek liner[14]. These measurements have also shown that the fluctuations of the measured parameters (rise and fall times, voltage amplitude, and charge) are not larger than about $\pm 10\%$ of their mean value. These results were supported by GEANT [15] simulations, performed previously[16, 17].

In addition to the response to fast muons, the response of the WCD to fast electrons and gamma-rays was obtained. Both, electrons and gamma-rays, produce also an amount of light proportional to their track lengths. It should be taken into account that gamma-rays are detected through their interaction with the water going essentially through pair-creation processes. This is the most probable case, given the relative cross sections at the typical gamma-ray energies present in the EAS. Therefore, the signals produced by gamma-rays are roughly the same as those produced by fast electrons, provided their energy distributions are similar (see Figure 8).

It should be taken into account that the signal produced by a muon with energy higher than ~ 400 MeV becomes indistinguishable from the signal produced by an electron with energy higher than ~ 250 MeV [18]. Hence, these values were used to normalize the signals from electrons to those corresponding to muons.

In order to include in the simulations the effect of the signal distortions in the cables, we have recorded in a previous work the average pulse shape for vertical muons transmitted through 200 m of RG-213 cable.

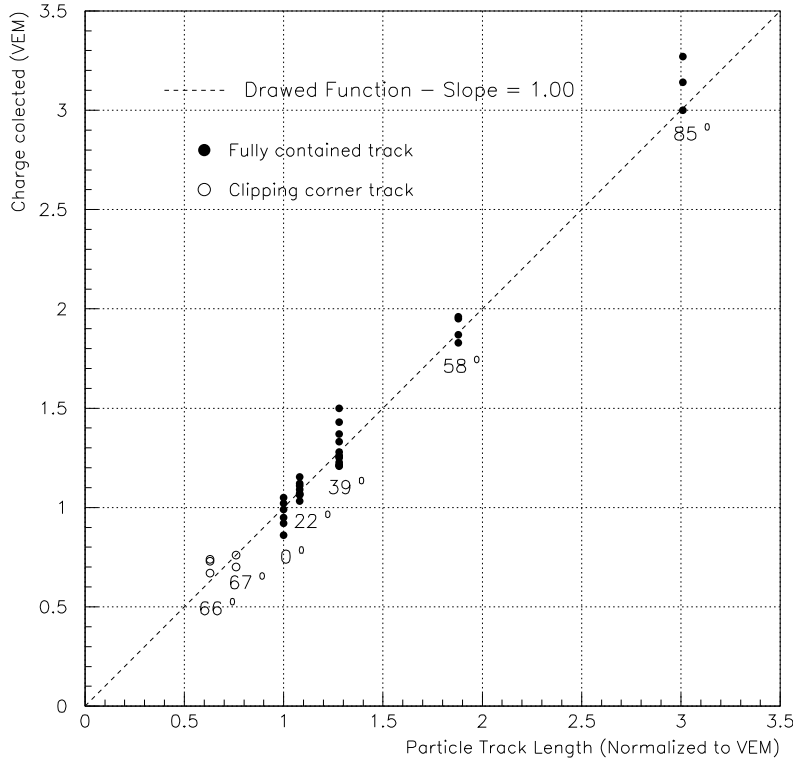


Figure 9: Sum of the charges collected in the three PMTs as a function of the particle track length in the detector water. The muon zenithal angles are also indicated. The identity function was drawn for comparison purposes. See text for details.

By taking into account all this information, the simulation of the surface detector signal was carried out as described below:

- **Muons:** For each muon hitting a detector station, a zenithal angle is selected using a gaussian-shaped random number generator, with its mean value centered in the zenithal angle of the primary particle of the EAS, and a sigma value of 4° . Hence the particles are restricted to an angular range of about $\pm 25^\circ$ [18]. Once the zenithal angle is established, the range of the particle in water is obtained according to its energy, and a peak amplitude is found as a function of its range. If the range of the muon exceeds the track length inside the surface detector, then the amplitude is made proportional to the track length. Finally, rise and fall times are selected with a gaussian shaped random number generator and the pulse shape is written to memory, considering the respective time delay from the AIRES results (again conveniently spread using a gaussian random number generator). The signal peak amplitudes, as well as the rise and fall times, are established also from gaussian-shaped random number generators, with their relative sigma-values obtained from measurements.
- **Electrons:** The general procedure is similar to that described for muons. The main difference occurs in the calculation of the range, which, in the case of the electrons,

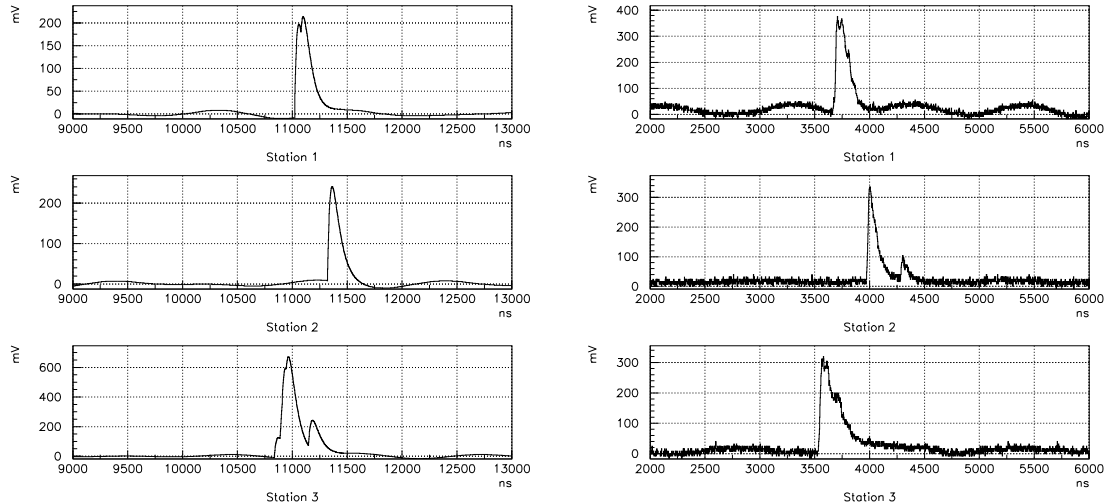


Figure 10: Simulated event (left) and pulses recorded from a real coincidence event detected in the three large WCDs (right). Both events were chosen arbitrarily and are shown only for comparison. The overall zero time for the simulated event is arbitrary and uncorrelated with the zero time for the measured one. Note the simulated noise pick up and the different vertical scales (adjusted automatically by the plotting program).

is assumed to be completely contained within the WCD, *i.e.* no backscattered electrons are simulated. The values of the peak amplitudes are obtained from electron simulations performed previously using the program GEANT.

- **Gamma Rays:** The energy of the γ -rays originated in an EAS range from ~ 10 MeV to ~ 100 MeV, and the main interaction channel in water goes through the pair creation process. In this energy regime, the mean interaction length of gamma-rays in water is about 80 cm. The track length for a specific gamma-ray (which depends on the zenithal angle selected as described above), determines the probability of creation of an electron-positron pair. In this case the electron simulation routine is called with two electrons, having a total energy balancing the gamma-ray energy. The energy of the recoiling nucleus is neglected.

The resulting final program is very fast; once the ARIES tables are locally available in a 233 MHz PC running under Linux, it simulates an average of 100 events/minute, and produces realistic pulse shapes as shown in Figure 10, where a real shower is compared with a simulated one.

As a summary, we have simulated the output of the digitizing electronic stage, reproducing the detector signal on the basis of previously known parameters relating the underlying physics with the detector response. The effect of the cables on the signal shape and the influence of the pick-up noise (only for the AM band), have been considered.

4 Shower Reconstruction

The reconstruction of the showers aims to find the direction of the shower axis, and to make an estimation of the energy of the primary cosmic ray. This reconstruction could be made in principle by performing a careful evaluation of a number of parameters which are measured from the oscilloscope traces, and from a comparison with the results of the simulations.

The reconstruction procedure is initiated by the obtention of the direction of the shower axis by fitting the arrival times to each detector, assuming a flat shower front. Once the direction is determined, the core position is found through minimization of the lateral distribution function using the particle density falling over each station. Then, using Monte Carlo simulations, it is possible to correlate the shower primary energy with the particle density measured by the detector stations.

4.1 Reconstruction of the shower direction

The reconstruction of the direction is based on the arrival times of the shower front particles to each detector station in the array. In order to determine the “trigger time” in each station, the voltage signal is time-integrated, and the crossing times of charge amplitude values equal to 10%, 50% and 90% of the maximum collected charge are determined, with the condition that no dynamic range saturation occurs. These times are called t_{10} , t_{50} and t_{90} , respectively. These parameters behave like constant fraction discriminators crossing times, and they are valuable for the comparison of the overall time structure of the station’s signals when different particle densities are measured.

The t_{10} are good indicators of the arrival time of the shower front to the detectors and they are used to obtain the shower axis direction, which is coincident with the primary cosmic ray arrival direction. On the other hand, the t_{50} and t_{90} are more closely related with the time structure and temporal width of the shower than with the shower direction, and can be used to estimate the primary mass composition and also the core distance [22, 23].

If three ground stations detect a shower, its axis can be determined by triangulation with reference to the arrival times and to the positions of the stations. This is made by searching for a unique, downward-going shower front, which we assume to be a plane, and moves at the speed of light. When all four detectors are hit, then a least squares method is used to find the best fit to this plane shower front. More elaborate and detailed algorithms can be used to obtain the shower direction including, for instance, the radius of curvature of the shower front. However, if we use the available data obtained from our four stations and try to use more complicated algorithms they, very often, fail to converge.

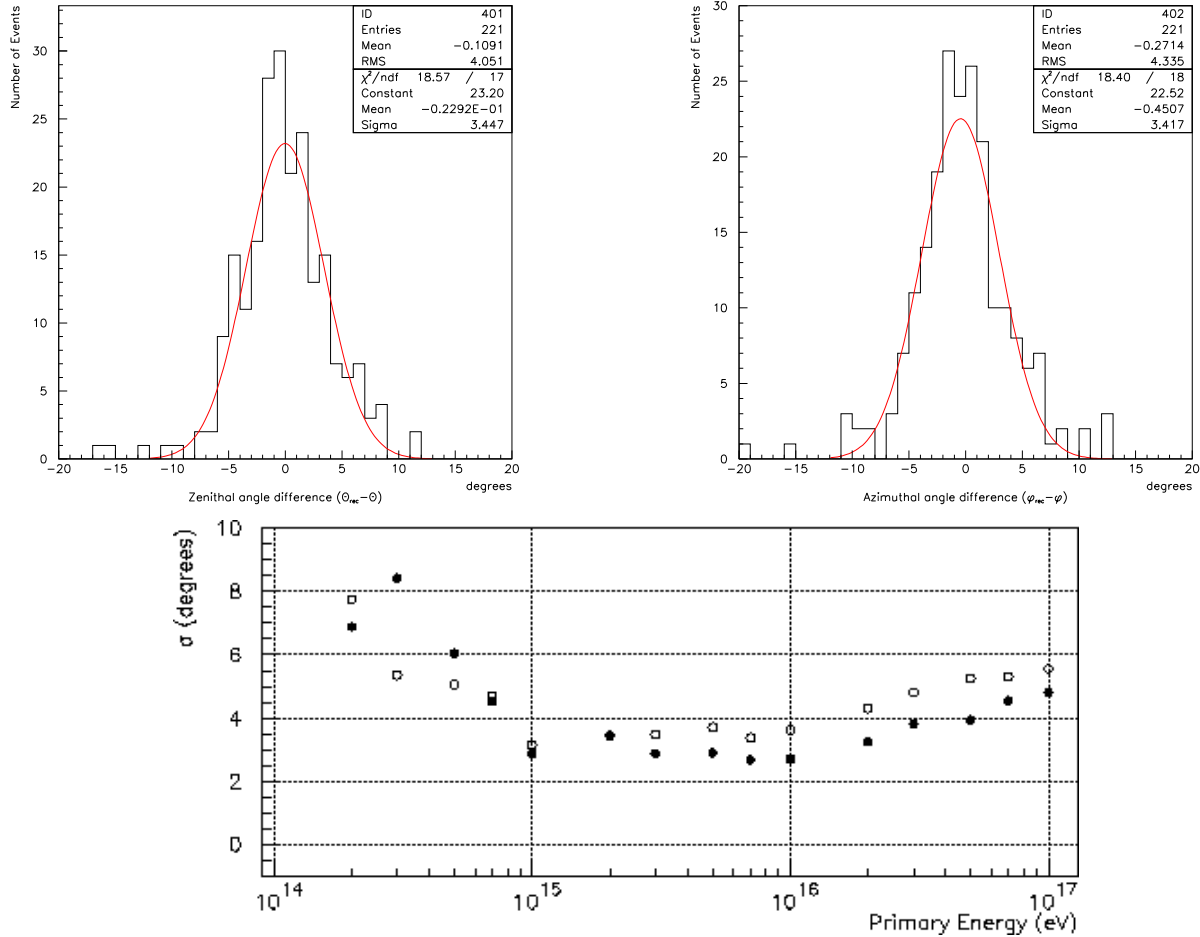


Figure 11: Typical gaussian fit to reconstructed zenithal and azimuthal angles. The energy dependence of the angular resolution (σ) is also shown. Filled dots correspond to azimuthal angle and open dots to zenithal angle.

4.1.1 Angular resolution

As described above, the t_{10} values were obtained from the simulated events database and used to obtain the arrival direction of each event. From this reconstruction the θ and ϕ , (zenithal and azimuthal angles) were obtained. These angles are the spherical angular components of a vector, normal to the (assumed) plane shower front. The accuracy in the reconstruction is determined by comparing these angles with the “true” angular direction of the particular simulated event, which is read from the events database.

As can be seen in Figure 11, the angular resolution (σ) of the array improves progressively with energy in the decade of 10^{14} eV, then remains almost constant in the decade 10^{15} eV and slowly decreases beyond $\sim 10^{16}$ eV.

The reconstructed plane is, actually, a plane parallel to the plane tangent to the shower curved front surface crossing the array at its center point. Beyond $\sim 10^{16}$ eV the shower front

disk is much larger than the geometrical size of the array and the probability of having the shower core falling away from the array, and being still able to produce a trigger, is higher than the probability for the core to fall closer. Because of the finite radius of curvature of the shower front, the vector normal to the tangent plane is more tilted, respect to the shower axis, at points lying far away from the core than for points closer to the core.

Typical shower front curvature radius are in the order of 10 km, hence at a distance of 300 meters from the geometrical center of the array, the normal to the tangent plane is tilted $\sim 2^\circ$ respect to the shower axis. This angular difference between the shower axis and the reconstructed direction have to be added to the intrinsic angular resolution of the array, which is of the same order of magnitude. This effect might explain the decrease in angular resolution at higher energies. Also, this may be interpreted as an energy limit for the validity of the flat shower front assumption, given the size of our array.

4.2 Reconstruction of shower energy

The axial symmetry assumption for an EAS is relevant for the energy analysis. It means that in a plane perpendicular to the shower axis, the particle density only depends on the radial distance from the axis. On the ground plane this symmetry is lost (unless the shower is vertical). However, for moderate zenithal angles ($\leq 40^\circ$) the assumption of a symmetric distribution is a valid approximation. For instance, if the EAS has a zenithal angle of 40° and the shower front has a diameter of 300 meters (typical size of the TANGO array) the forward component of the shower front travels about 250 meters more than the backward component to reach the ground. Considering the measured attenuation length reported in the Haverah Park experiment of (780 ± 35) gr/cm²[19], the forward component of the shower front would be attenuated only $\sim 5\%$ with respect to the backward component. This calculation shows the validity of the approximation. On this basis, we assume in the following that axial symmetry is a valid assumption.

A key parameter required to estimate the energy of an EAS is the LDF, *i.e.* the particle density as a function of the distance to the core position. From the results of previous experiments [20, 21] it is possible to propose the functional dependence:

$$\rho = \frac{A}{r^{\eta+r/r_0}} \quad (1)$$

where ρ is the particle density ([VEM/m²]), r is the distance to the core ([m]), A is a normalization constant (proportional to the primary particle energy) and η and r_0 control the shape of the LDF. The last two parameters were obtained by fitting the previous expresion to simulated particle density distributions, which have included the detector response to different shower particle species (μ^\pm , e^\pm and γ -rays) as described in 3.2.1.

Figure 12 shows the fits using Equation 1 to the simulated particle densities “measured” with the simulated WCD for several primary energies, where all zenithal angles included in

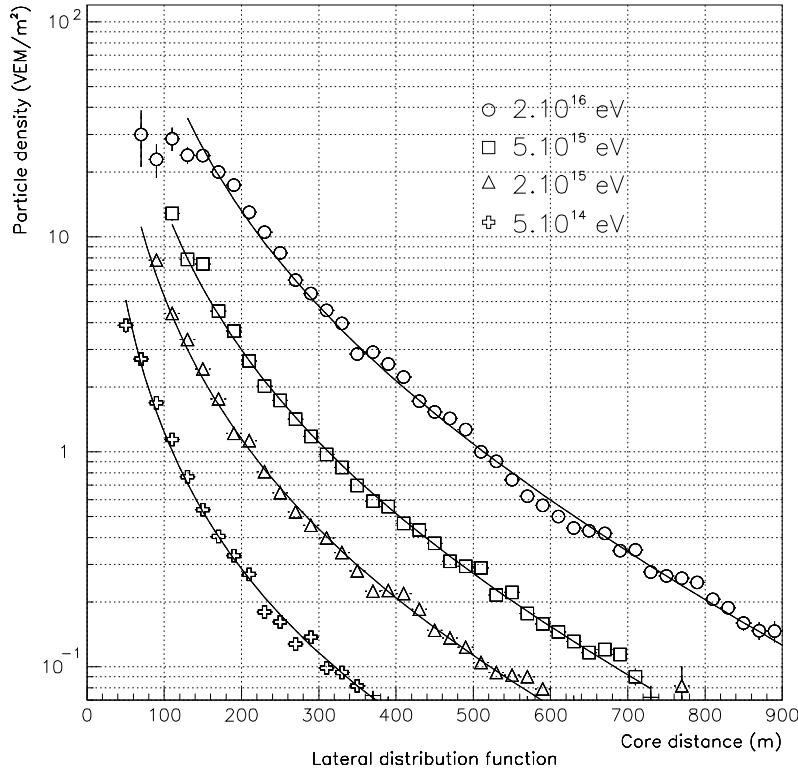


Figure 12: Fits to the averaged simulated lateral distribution function for different proton primary energies. The zenithal angles has been averaged in each core distance bin.

the simulation were averaged within each core-distance bin. The small “plateau” observed in the leftmost part of the 2.10^{16} eV curve is produced by the (simulated) electronic dynamic range saturation.

It should be noted that the η parameter is slightly sensitive to the primary particle mass [24] as was found by fitting the previous expresion to the simulated data events. The reproduction of such dependence from simulations is an encouraging result. Although different approaches were attempted to obtain, at least, a primary mass indicator from the reconstructed events in the simulated database, none of them were satisfactory, probably due to the simulated shower-to-shower fluctuations that might mask the small differences in the η

	η	r_0
Proton	1.99 ± 0.02	3400 ± 150
Iron	1.94 ± 0.02	3400 ± 100
Average	1.965	3400

Table 1: Lateral distribution function parameters obtained from the simulated events database for both primary species. Also, the average values used in the reconstruction algorithm are shown.

parameter for different primary species. Because of this we used in the following an average value for the η parameter between the values corresponding to proton and iron primaries (see Table 1).

It is known from extensive Monte Carlo simulations[20] that there exists a certain distance from the shower core for which the particle density of an EAS correlates with its primary energy and also their fluctuations are minimized. In the present experiment performed with only 4 detectors, we have used a simplified model where the normalization constant A of LDF was correlated with the primary energy instead of the particle density at a fixed distance of the core position. The LDF was obtained from particle density measurements in each detector station, far away from the core.

The normalization constant of the LDF is found through minimization of the following equation

$$\chi^2 = \sum_{i=1}^n \left(\rho_i - \frac{A}{r_i^{\eta+r_i/r_0}} \right)^2 \quad (2)$$

where ρ_i and r_i are the particle density and the distance between the core impact position and the i -th station, respectively, and η and r_0 were obtained from simulations as mentioned before. Finally, the particle density measured by each station is obtained by the ratio of the time-integrated oscilloscope trace (bias subtracted) and the VEM value corresponding to that particular detector station. This ratio yields the number of equivalent particles falling in the station. Then, the equivalent particle densities (VEM/m^2) is obtained by simple normalization to the respective detector area.

The minimization of Equation 2 was performed through a grid search on the simulated data of the events database, yielding the x and y coordinates of the core position, as well as the normalization constant A . Table 2 shows the accuracy of the core position reconstruction obtained by this method for some energies. The accuracy is degraded at higher energies, probably because the shower front size becomes comparable with the array size.

Primary Energy	Core position accuracy
5.10^{14} eV	40 m
2.10^{15} eV	30 m
5.10^{15} eV	55 m
2.10^{16} eV	110 m

Table 2: Accuracy (RMS) of the reconstructed core position.

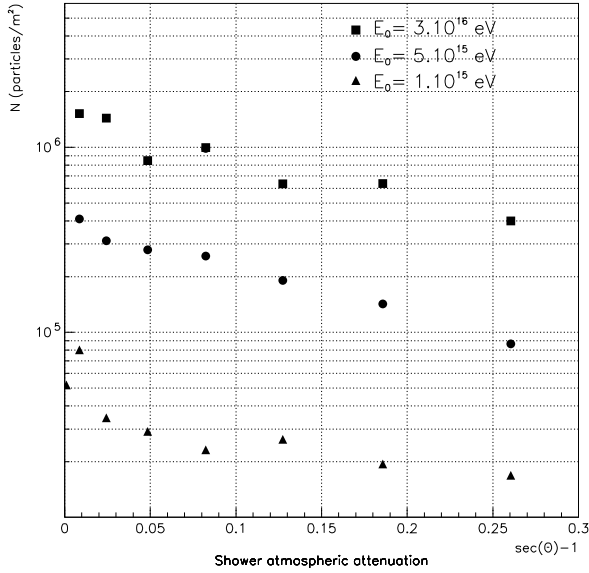


Figure 13: Simulated zenithal atmospheric attenuation for different primary energy.

4.2.1 Correction by atmospheric attenuation

The axial symmetry assumption proved to be a valid approximation regarding the forward and backward components of the shower front for non-vertical showers. However, the effect of atmospheric attenuation in a tilted EAS development cannot be ignored. In order to get an evaluation of the magnitude of this effect we used the simulated events database to estimate the atmospheric attenuation on the shower propagation through the atmosphere.

By simple geometrical considerations it is possible to propose a functional dependence of the form

$$N = Ae^{[\beta(\sec(\theta)-1)]} \quad (3)$$

where N is a normalization factor, proportional to the primary particle energy that includes the atmospheric attenuation correction factor and this constant includes the atmospheric attenuation correction factor.

For each primary energy, the simulated showers were divided in zenithal angle bins of 5° each, and a fit was performed to the data using the functional dependence shown in Equation 3, *i.e.*, assuming only a dependence for the A parameter on the zenithal angle. The average value obtained for β by fitting the simulated data to Equation 3 is $\beta = 4.1 \pm 0.1$. For the zenithal range of interest ($\theta \leq 30^\circ$) this correction because of the atmospheric attenuation increases the estimated EAS's energy up to $\sim 50\%$.

4.2.2 Primary energy assignment

Finally, after minimization of Equation 2 and being performed the atmospheric attenuation correction (for which the directional reconstruction is required) it is possible to show the relationship between N -a parameter obtained from the shower reconstruction routine- and the primary energy (obtained from the simulated events database). It should be noted that in this survey over the simulated events database we found that, beyond $\sim 2.10^{16}$ eV, N fails to converge, and the linearity (in logarithmic scale) as a function of the primary particle energy is lost. Therefore, only data at lower energies are shown in Figure 14.

From these fits we obtain the following expressions, useful to correlate the parameter N [VEM/m²] with the primary energy [eV]:

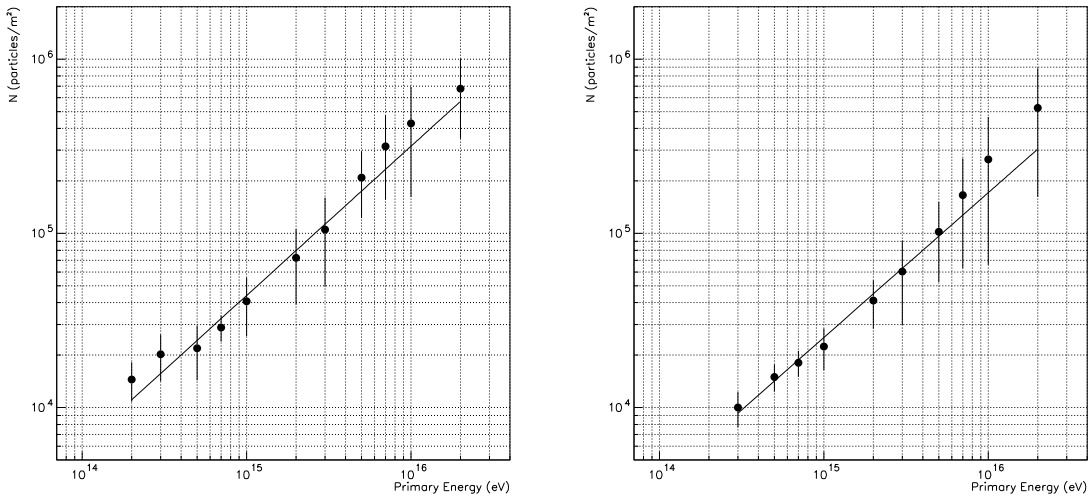


Figure 14: Relationship between N and primary energy. Left: proton primary. Right: iron primary.

$$E_0 = (4 \pm 1)10^9 N^{1.17 \pm 0.03} \quad (4)$$

and

$$E_0 = (5 \pm 2)10^9 N^{1.20 \pm 0.03} \quad (5)$$

where Equations 4 and 5 correspond to proton and iron primaries, respectively.

From these equations it is possible to estimate the relative error in the energy reconstruction. Even when the expression has a dependence on the N value, its dependence is logarithmic, and the $\Delta N/N$ value was found to be ~ 0.4 from the simulated database. This yields a relative error of 57% and 66% for protons and iron nuclei, respectively, in the energy range from $\sim 10^{14}$ eV to $\sim 10^{16}$ eV.

According to these results, a knowledge of the primary particle mass would be required to correctly correlate the N parameter with the primary particle energy by choosing the proper expresion. Strictly, this fact prevents us to make an unambiguous assignment of the primary energy. Furthermore, it should be recalled that both Equations 4 and 5, were obtained from surveys performed on the Monte Carlo simulations, which are dependent of the particular hadronic package utilized. On the other hand, however, the results obtained from both expresions are consistent within errors.

5 Summary

A new, Extended Air Shower Array has been constructed in Buenos Aires during 1999 and was commissioned in 2000. It consists of 4 Water Čerenkov Detectors, three of them are arranged in a triangular shape and the fourth is near the center of the triangle. The enclosed area is $\sim 30.000 \text{ m}^2$. The detectors placed in the vertices of the triangle have a footprint area of 10 m^2 , the central detector has 0.5 m^2 .

Detailed Monte Carlo simulations of the showers were performed using the AIRES code with the SYBILL hadronic package. Various computer programs and routines were developed to simulate the array response including the surface detector, front end electronics, pick-up noise, and triggering. It should be noted that an effort was made to use experimental data whenever possible. The simulated events database contains a total of 360000 events.

A reconstruction routine has been developed from the simulated shower database. According to the simulations, the angular reconstruction resolution is better than 5° in the range $5 \cdot 10^{14} \text{ eV}$ to 10^{17} eV . The accuracy expected in the energy resolution is roughly 60% in the range $\sim 10^{14} \text{ eV}$ to $\sim 10^{16} \text{ eV}$. With respect to the primary mass determination it is concluded from the present simulations that no unambiguous assignment can be made, at present, from the showers measured with our array.

A fully automatic system for calibration, monitoring and data acquisition has been built using standard NIM and CAMAC modules and a 4-channel digital oscilloscope connected to standard PCs. Data have been continuously collected since September, 2000 and the shower reconstruction analysis will be published in an forthcoming paper.

6 Acknowledgements

We are very especially indebted to the late J.Vidallé for his unvaluable dedication and help in the early stages of the TANGO Array.

We are also deeply indebted to D.Simoncelli and E.Fisher for their outstanding work at the Mechanical Workshop in TANDAR Laboratory. Also, we would like to express our gratitude to P. Stoliar, H. Di Paolo, C.Bolaños, J.Fernández Vásquez and O.Romanelli, for their help with different aspects of the electronic system. Thanks are given to M.Figueroa and M.Wagner for their work in the characterization of the PMTs. We would like to mention H.Grahmann, O.Ruiz, E.Altmann, A.Ferrero and A.Etchegoyen. They helped us in many different ways. We also thank Prof. Ma Yu Quian, from Beijing University, for the donation of the 3-inch PMT used in the central detector and to *Plásticos Industriales S.A.*, specially E.Carricundo and P.Martelli for the donation of the fiberglass-reinforced tank. Finally, we would like to thank Fermilab for the loan of some electronic modules used in the experiment (Fermilab Loan C96082).

The work of P. Bauleo, C. Bonifazi and A. Reguera was supported by different CNEA fellowships. This work was partially supported by a CONICET grant (PIP 4446/96).

References

- [1] P. Bauleo *et.al*, Nucl. Inst. and Meth. A406,69 (1998)
- [2] The Auger Collaboration *Pierre Auger Project Design Report*, Revised Edition, March, 1997
- [3] R. Atkins, *et.al* The Milagro Collaboration, Nucl. Inst. and Meth. A449, 478 (2000)
- [4] A. Filevich *et.al*, Nucl. Inst. and Meth. A423,108 (1999)
- [5] O. Bernaola *et.al*, GAP-1996-036
- [6] D. Ravignani *et.al*, GAP-1997-024
- [7] T. Kutter *et.al*, GAP-1997-025
- [8] P. Bauleo *et.al* accepted for publication in NIM, and GAP-2000-027
- [9] J. Rodríguez Martino *et.al*, GAP-1997-032
- [10] S. Sciutto, The AIRES program is available at
<http://www.fisica.unlp.edu.ar/auger/aires>
- [11] D. Ravignani *et.al*, GAP-1996-020
- [12] C. Walck, Private Communication.

- [13] C. Bonifazi, *et.al.*, Lic. Thesis (Buenos Aires University), and GAP note to be submitted
- [14] F. Hasenbalg *et.al.*, GAP-1997-027
- [15] GEANT, CERN Program Library
- [16] FCEN & TANDAR Groups, GAP-1996-011
- [17] P. Bauleo *et.al.*, GAP-1996-029
- [18] C. Pryke, Ph.D. Thesis, Leeds University (1996)
- [19] D.M. Edge *et.al.*, J. Phys. A, 6, 1612 (1973)
- [20] M. Lawrence *et.al.*, J. Phys. G, 17, 733 (1991)
- [21] H. Dai *et.al.*, J. Phys. G, 14, 793 (1988)
- [22] J. Linsley, J. Phys. G, 12, 51 (1986)
- [23] A.A. Watson *et.al.*, J. Phys. G, 7, 1199 (1974)
- [24] The Auger Collaboration *Pierre Auger Project Design Report*, Revised Edition, p. 86, March 1997

Note: The *Pierre Auger Project Design Report* and the Pierre Auger Project Internal Notes (GAPs) can be found in:

<http://www.auger.org/admin/index.html>